Editors' Suggestion

Measuring the Local Velocity along Transition Paths during the Folding of Single Biological Molecules

Krishna Neupane, Noel Q. Hoffer, and M. T. Woodside
Department of Physics, University of Alberta, Edmonton Alberta, T6G 2E1, Canada

(Received 14 December 2017; published 6 July 2018)

Transition paths are the most interesting part of folding reactions but remain little studied. We measured the local velocity along transition paths in DNA hairpin folding using optical tweezers. The velocity distribution agreed well with diffusive theories, yielding the diffusion coefficient. We used the average velocity to calculate the transmission factor in transition-state theory (TST), finding observed rates that were $\sim 10^5$-fold slower than predicted by TST. This work quantifies the importance of barrier recrossing events and highlights the effectiveness of the diffusive model of folding.

DOI: 10.1103/PhysRevLett.121.018102

Transition paths are the part of a reaction spent crossing the energy barrier between reactants and products [1–3]. In the context of biomolecular folding reactions, the reactants and products are the folded and unfolded states of the molecule (Fig. 1). Transition paths represent the most interesting part of the trajectories in folding reactions because they encapsulate all the key information about folding mechanisms: the high-energy transition states in the barrier region that are occupied during the transition paths dominate the kinetics of the folding and define the mechanism. Transition paths are very difficult to measure experimentally, however, owing to their brief duration, typically on the μs scale and hence 1000- to 1×10^6-fold (or more) shorter than the lifetime of the unfolded or folded states, posing technical challenges for the single-molecule measurements that are required to observe them. As a result, they have not been experimentally accessible until recently [4].

Improvements in single-molecule methods have now allowed transition-path properties to be measured directly [5–11]. To date, these studies have focused primarily on the time required for the transition to take place: the average transition-path time has been measured for both proteins [5–9] and nucleic acids [10,11] using advanced single-molecule fluorescence and force spectroscopy methods, and the variations in time for individual transition-path crossings have been measured in proteins and nucleic acids with force spectroscopy [12,13]. In many ways, however, the local velocity along the transition paths is more interesting than global properties like the transit time. The velocity reflects the dynamics within the crucial transition states, a feature of folding reactions that has not been possible to observe previously. Furthermore, measuring local variations in the transition paths provides the most fine-grained experimental description that can be achieved of the microscopic motions a molecule undergoes while folding. Here we report the first measurements of transition-path velocities, studying the folding of DNA hairpins as a model system for "two-state" folding with optical tweezers-based force spectroscopy [14]. We characterized the properties of the local velocity along the transition paths and related them to the physical picture of folding as a diffusive search over an energy landscape [15–17].

Single DNA hairpins having different sequences and energy landscapes (specifically, hairpins 20R0/T4, 20R25/T4, 20R55/T4, 20R100/T4, and 30R50/T4 from Ref. [18] and 20TS06/T4 from Ref. [19]) were attached to beads held in high-resolution optical traps via kilobase-long linkers of double-stranded DNA [Fig. 2(a), upper inset] as described [18] (see Supplemental Material [20]). Hairpins were held under tension near $F_{1/2}$, the force at which the folded and unfolded states were equally occupied, at constant trap separation. The end-to-end extension of the molecule was measured as the hairpin fluctuated in equilibrium between folded and unfolded [Fig. 2(a)], yielding a total of ~8500–46 000 transitions for each

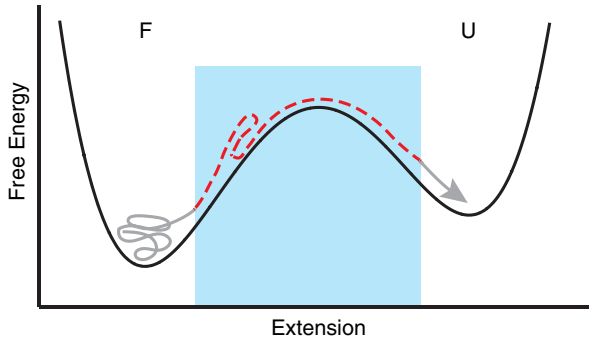

FIG. 1. Transition paths in folding reactions. A transition path (dashed line) represents the part of the trajectory (gray) that crosses the energy barrier (shaded region) separating the folded (F) and unfolded (U) states.

hairpin. High trap stiffness (0.75–1.1 pN/nm in one trap, 0.56–0.63 pN/nm in the other) was maintained to maximize the time resolution of the measurement; under these conditions, the time resolution of the measurement was 6–9 μs [13], and the kinetic artifacts from beads and handles [27] were small [28]. Transition paths were identified from the extension trajectories [Fig. 2(b)] as those parts of the trajectory passing between two boundaries (x_1 and x_2) demarking the barrier region. In order to capture as much of the dynamics between the folded (F) and unfolded (U) states as possible, the barrier region was defined as the middle 2/3 of the distance traversed between F and U. We found the velocity of the transition paths $v(t)$ from the local slope of the trajectory $x(t)$. To reduce the effects of random measurement noise, the trajectories [Fig 2(b), black] were first smoothed with a smoothing spline interpolation [Fig. 2(b), red] before numerical differentiation [Fig. 2(b), upper inset] [20]. The velocity at each position along the reaction coordinate $v(x)$ was then found directly from the curve $v(t)$ as it crossed each x value, allowing $v(x)$ to be multivalued wherever recrossing events occurred within a trajectory.

The velocity showed distinct local variations as the molecule crossed the barrier region, reflecting complex dynamics within the transition states. In some transitions the motion was fast across the whole barrier [Fig 2(c), left], but in others the fast motions were interrupted by periods of slower motion [Fig 2(b)] and even transient reversals in the direction of motion [Fig 2(c), center and right]. Episodes of fast, slow, and reversed motion were distributed roughly randomly along transition path from one transition to the next. Indeed, the distribution of velocity as a function of position within the barrier region measured from all transitions for each hairpin [Figs. 3(a) and S1(a)] showed velocities ranging from roughly −0.5 to 1.5 mm/s at all positions. The overall distribution of velocities [Figs. 3(b)

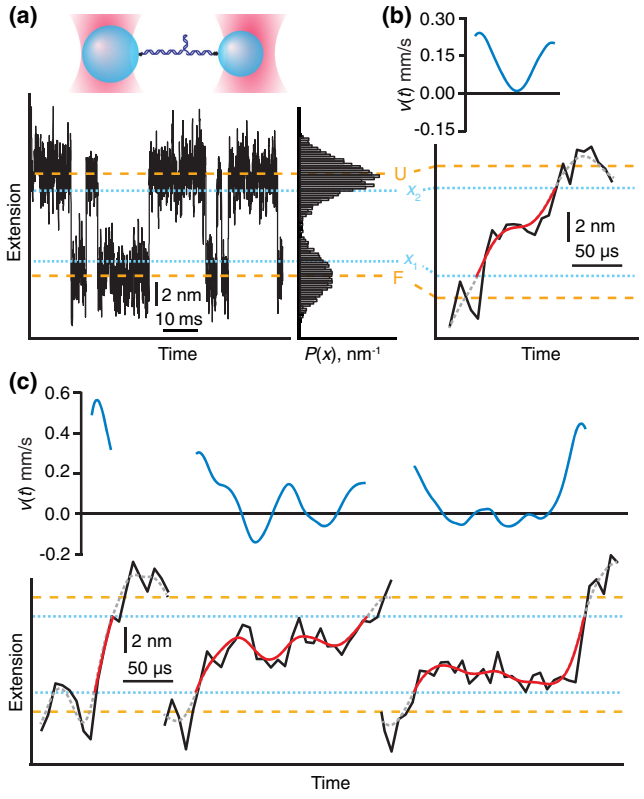

FIG. 2. Measuring transition paths in DNA hairpins with optical tweezers. (a) The end-to-end extension of the hairpin held under tension fluctuates between the folded and unfolded states (dashed lines). Upper inset: Cartoon of measurement. A hairpin attached to DNA handles is held between two beads trapped by laser beams. Right inset: Probability distribution of hairpin extension. (b) Zooming in on a single unfolding transition, the transition path is seen as that part of the trajectory crossing between the boundaries defining the barrier region (dotted lines). Inset: The velocity along the transition path is found by differentiating the smoothed transition path. (c) Selected unfolding transitions and corresponding velocity profiles showing a wide range of velocities. The trajectory sometimes reverses course along the transition path, reflecting barrier recrossing.

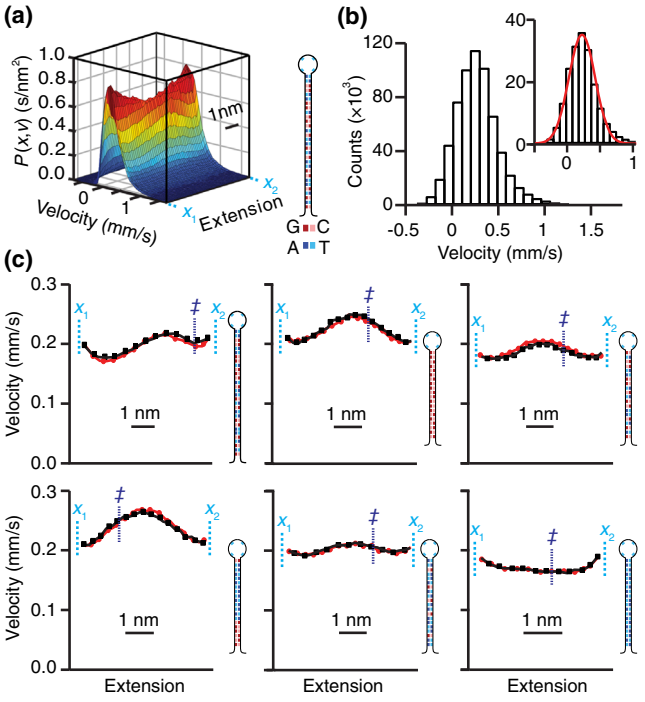

FIG. 3. Transition-path velocity distributions. (a) The probability density for the velocity as a function of position within the barrier region for the hairpin 30R50/T4. Inset: sequence of the hairpin 30R50/T4. (b) The distribution of velocities measured at all positions in the barrier region for the hairpin 30R50/T4 is close to Gaussian. Inset: Fitting the distribution of velocities observed at the barrier peak to a Gaussian yields D. (c) The average velocity profile within the barrier region is the same for folding (black) as for unfolding (red) but generally nonuniform. Cyan: barrier region boundaries (x_1, x_2). Blue: position of barrier peak (double dagger symbol). Insets: hairpin sequences. Error bars represent standard error of the mean.

and S1(b)] was close to Gaussian in all cases, but slightly skewed; for each hairpin, negative velocities indicating reversed motion were observed at every position within the barrier region, providing direct evidence of barrier recrossing events as expected for a diffusive process. Finding the average velocity profile along the transition paths from the mean of the distribution at each position in the barrier region, the result was the same for both folding [Figs. 3(c), black] and unfolding [Figs. 3(c), red] transitions, as expected from the time-reversal symmetry of the process. The velocity profiles varied by ~10%–40% across the barrier region and were noticeably different for different hairpin sequences. A similar analysis applied as a control to measurements of a reference construct consisting of handles without any hairpin, where the construct was abruptly stretched and relaxed [Fig. S2(a)] to generate extension changes similar to those seen during folding transitions [Fig. S2(b)], found a velocity profile with a ~threefold higher average velocity [Fig S2(c)] than seen with a hairpin present, indicating that the response of the bead was not limiting the measurement of the hairpin transition-path velocities.

We first considered what the transition-path velocity distributions reveal about the diffusion coefficient during folding, D. D is the crucial parameter that relates the kinetics of the folding to the thermodynamics of the energy landscape, reflecting the microscopic motions made by the molecule in its conformational search [15] and the "internal friction" that gives rise to speed limits in folding [29]. It is difficult to measure D using traditional approaches based on analysis of rates via Kramers' theory because of its exponential sensitivity to errors in barrier energies [8,11,30], but transition-path measurements provide a more sensitive and robust way to probe it [6,13,31]. Recent theoretical work showed that if a single type of transition path dominates the folding, then a 1D harmonic barrier will produce a Gaussian distribution of velocities at the barrier peak with average velocity

$$\langle v(x^{\ddagger})\rangle \approx 1.5D(\beta\kappa_b)^{1/2}, \tag{1}$$

where β is the inverse thermal energy and κ_b the barrier stiffness [32]. The barrier-peak location for each hairpin [Fig. 3(c), double dagger symbol] was taken as the average of the results found previously from the force dependence of the rates [18,19] and from energy-landscape reconstructions using committor analysis of the extension trajectories [13,33].

The velocity distribution at the barrier peak was indeed reasonably well fit by a Gaussian for each hairpin [Figs. 3(b), inset and S1(c)]. Calculating D from $\langle v(x^{\ddagger})\rangle$ via Eq. (1), we found good agreement with values for D obtained previously in independent ways: from the average transition path time (τ_{TP}) [12,13], from the exponential decay of the individual transit-time distribution [12,13], and from the folding rates via Kramers' theory [11] (Table I). The trend of increasing D with increasing G:C content found previously [13] was also recapitulated in the results from $\langle v(x^{\ddagger})\rangle$, enhancing confidence that the velocity measurements are reliable. In addition, the quantitative consistency of the results from four independent physical properties of the folding, each of which assumes a single dominant harmonic barrier and constant diffusivity, shows that these assumptions are reasonable, at least for DNA hairpins. They are not ideal, however, as suggested by the slight skew in the velocity distributions at $x^{\ddagger}$ (skew ~0.6–1.6). Indeed, Brownian-dynamics simulations of transition path trajectories [20] show that anharmonicity, position dependence of D, and the presence of multiple types of transition paths can all generate skew in the velocity distribution (Fig. S3). The observed skew likely reflects contributions from each of these effects, since the barriers are not strictly harmonic [13,19], D should vary at least somewhat with position [34,35], and 1D descriptions of hairpin folding are incomplete [36] even if they work reasonably well [37].

The average velocity profile $\langle v(x)\rangle$ shows even more substantial deviations from the theoretical expectations. For a dominant transition path with a 1D harmonic barrier $\langle v(x)\rangle$ is expected to have a minimum at the top of the barrier [32]. In most cases, however, the velocity is not near a minimum at the barrier top [Fig. 3(c)]. This disagreement could arise from anharmonicity in the barrier, reflecting the sensitivity of $\langle v(x)\rangle$ to the barrier shape as found previously in simulations [32], since energy-landscape

TABLE I. Comparison of D from $\langle v(x^{\ddagger})\rangle$, transition times, τ_{TP}, and rates. Results based on average transition time (τ_{TP}) and distribution of transition times ($P_{TP}(t)$) are from Refs. [12] and [13]. Results based on rates are from Ref. [11]. Errors represent standard error on the mean.

DNA hairpin	$\langle v(\ddagger)\rangle$ ($\times 10^2$ μm/s)	D from $\langle v(\ddagger)\rangle$ ($\times 10^5$ nm^2/s)	D from τ_{TP} ($\times 10^5$ nm^2/s)	D from $P_{TP}(t)$ ($\times 10^5$ nm^2/s)	D from rates ($\times 10^5$ nm^2/s)
30R50/T4	2.0 ± 0.3	2.5 ± 0.4	3.5 ± 0.3	1.8 ± 0.2	4.6 ± 0.5
20R100/T4	2.4 ± 0.2	3.1 ± 0.4	4.1 ± 0.3	2.2 ± 0.2	⋯
20R55/T4	2.0 ± 0.2	2.6 ± 0.5	3.6 ± 0.3	1.5 ± 0.2	⋯
20TS06/T4	2.5 ± 0.2	2.6 ± 0.7	3.1 ± 0.3	1.6 ± 0.2	5 ± 3
20R25/T4	2.0 ± 0.2	2.6 ± 0.5	2.6 ± 0.3	1.3 ± 0.2	⋯
20R0/T4	1.7 ± 0.3	2.2 ± 0.3	2.5 ± 0.2	1.0 ± 0.2	⋯

reconstructions show that the barriers are not completely harmonic [13,19]. Another possibility is that D is not constant (as assumed in the theory) but rather depends on position, as may arise from the projection of the full multidimensional landscape onto a 1D reaction coordinate [35]; a modest position dependence is also expected from the sequence dependence of diffusion in DNA duplexes [13]. The likely influence on $\langle v(x)\rangle$ of the position dependence of D can be deduced by comparing the experimental velocity profiles to those obtained from Brownian dynamics simulations of transitions over the energy landscapes measured for each of the hairpins [13,19] made under the assumption of a constant D. Although $\langle v(x)\rangle$ from the simulations (Fig. S4) recapitulates some of the qualitative features observed experimentally [Fig. 3(c)], the details of the spatial variations differ, suggesting that at least some of the variations come from position dependence of D.

An intriguing aspect of transition-path velocities is that they illuminate the role of barrier recrossing events in folding reactions, by showing how recrossing alters the observed rates and velocities from what would be expected if instead classical transition-state theory (TST), which neglects recrossing, held true. In TST, the microscopic velocity is the thermal velocity of the molecule, $v_{\mathrm{th}} = (2k_BT/\pi m)^{1/2}$, where m is the mass. If barrier recrossing does not occur, then the rate should be related to the velocity across the barrier by

$$k_{U/F}^{\mathrm{TST}} = P(x^{\ddagger})v_{\mathrm{th}}/2P_{F/U}, \tag{2}$$

where $k_{U/F}^{\mathrm{TST}}$ is the transition-state theory rate for unfolding or refolding, $P(x^{\ddagger})$ is the Boltzmann-weighted equilibrium occupancy at the barrier peak, and $P_{F/U}$ is the fractional occupancy of the folded or unfolded state [2,38]. If barrier recrossing does not occur frequently, then the observed rates ($k_{U/F}$) should be similar to $k_{U/F}^{\mathrm{TST}}$. However, if recrossing events are significant then one would expect $k \ll k^{\mathrm{TST}}$; the transmission factor $\kappa = k/k^{\mathrm{TST}}$ quantifies the importance of recrossing as the factor by which the rates are depressed compared to TST. The transmission factor can also be determined from the velocity, using relations between the observed velocity, the probability distribution along the transition paths, and the committor probability [32,39]:

$$\kappa = \langle v(x^{\ddagger})\rangle/2v_{\mathrm{th}}. \tag{3}$$

We evaluated κ from both the rates and the velocities. First, the rates $k_{F/U}$ were determined from single-exponential fits (Fig. S5) to the distributions of unfolded- or folded-state lifetimes, as measured directly from the extension trajectories by partitioning the trajectories into the two states via thresholding [18], $P_{F/U}$ was found from the fraction of time spent in each state, and $P(x^{\ddagger})$ was evaluated from the free-energy landscape via $P(x^{\ddagger}) = A\exp(-\beta\Delta G^{\ddagger})$, where A is the normalization constant ensuring $\int P(x)dx = 1$. The thermal velocity was calculated (Table S1) by estimating m as the mass of the part of the hairpin remaining unfolded when the barrier was crossed at $x^{\ddagger}$ [20]. The TST rates implied by Eq. (2) were found to be much higher than the rate observed directly in the extension trajectories for every hairpin (Table S1), by a factor of roughly 100 000-fold, yielding $\kappa \sim 10^{-5}$ (Table II). The values for κ obtained independently from the velocities via Eq. (3) were in excellent agreement with those found from the rates (Table II).

TABLE II. Comparison of κ from rates, velocities, and Kramers' theory. Errors represent standard deviation.

DNA hairpin	κ from rates ($\times 10^{-6}$)	κ from velocities ($\times 10^{-6}$)	κ from Kramers' theory ($\times 10^{-6}$)
30R50/T4	10 ± 4	10 ± 2	11 ± 2
20R100/T4	10 ± 1	9 ± 2	9 ± 1
20R55/T4	7 ± 1	7 ± 2	7 ± 2
20TS06/T4	4.4 ± 0.4	7 ± 3	7 ± 2
20R25/T4	5.4 ± 0.5	7 ± 2	7 ± 2
20R0/T4	0.9 ± 0.2	6 ± 2	5 ± 1

These results indicate that barrier recrossing plays a central role in folding transitions, reducing rates by ~5 orders of magnitude. Classical transition-state theory thus does not provide a good description of folding and using it to estimate kinetic prefactors or activation energies as sometimes done [40] will lead to substantial overvaluation. Instead, diffusive theories like Kramers' approach or its generalizations [30] are more appropriate. In fact, κ can be evaluated directly from Kramers' theory as $\kappa = (m\kappa_b)^{1/2}\beta D$ [30]. Using the average values of D from Table I, we obtained very similar values for κ as found from the rates and velocities (Table II). Although it has previously been shown that Kramers' theory accounts well for the observed kinetics in both simulations [41–43] and experiments [8,44,45], the transmission factor reflecting the influence of barrier recrossing has not previously been measured.

More generally, this study of the velocity in transition paths highlights how well the diffusive model of folding reactions works to describe and predict folding phenomena. Remarkable quantitative consistency is seen across a wide range of experimental observables at various scales. Analyzing different kinetic properties of folding, for example, leads to consistent values for the diffusion coefficient whether looking at rates [11], the much-smaller transition times [12,13], or the speed of motion along the transition paths. The statistics of transition-path occupancy also quantitatively match what is expected for diffusive motions over the energy landscape [37,46], whether reconstructed under equilibrium or nonequilibrium conditions [19,33,47]. Finally, kinetic models of unfolding-force

distributions based on diffusive theories [48,49] not only capture the shape of the distribution but also yield values for the energy-barrier location and height that agree with model-independent reconstructions of the landscapes [8,19,33] as well as rate values that agree with those measured directly [11]. This consistency across numerous observables and many different types of measurement gives strong confidence in the quantitative validity of the diffusive picture of folding.

The measurements of local variations in the transitions paths demonstrated here open many new possibilities for studying folding. For example, variations in the velocity should allow the local energy landscape roughness, reflecting localized changes of internal friction in the molecule, to be deduced. Cataloguing the different types of transition-path shapes observed should also allow the identification and characterization of different classes of transition paths crossing different barriers, probing directly the competition between pathways that underlies the statistical view of folding. Transition-path studies promise to be an exciting new frontier in the science of folding.

The authors thank D. E. Makarov and G. Hummer for helpful discussions, and A. G. T. Pyo for providing code for the simulations. This work was supported by the Natural Sciences and Engineering Research Council Canada and Alberta Innovates.

N. Q. H. and K. N. contributed equally to this work.

[1] P. G. Bolhuis, D. Chandler, C. Dellago, and P. L. Geissler, Annu. Rev. Phys. Chem. **53**, 291 (2002).
[2] G. Hummer, J. Chem. Phys. **120**, 516 (2004).
[3] W. E and E. Vanden-Eijnden, Annu. Rev. Phys. Chem. **61**, 391 (2010).
[4] H. S. Chung, J. Mol. Biol. **430**, 409 (2018).
[5] H. S. Chung, K. McHale, J. M. Louis, and W. A. Eaton, Science **335**, 981 (2012).
[6] H. S. Chung and W. A. Eaton, Nature (London) **502**, 685 (2013).
[7] H. S. Chung, S. Piana-Agostinetti, D. E. Shaw, and W. Eaton, Science **349**, 1504 (2015).
[8] H. Yu, A. N. Gupta, X. Liu, K. Neupane, A. M. Brigley, I. Sosova, and M. T. Woodside, Proc. Natl. Acad. Sci. U.S.A. **109**, 14452 (2012).
[9] H. Yu, D. R. Dee, X. Liu, A. M. Brigley, I. Sosova, and M. T. Woodside, Proc. Natl. Acad. Sci. U.S.A. **112**, 8308 (2015).
[10] K. Truex, H. S. Chung, J. M. Louis, and W. A. Eaton, Phys. Rev. Lett. **115**, 018101 (2015).
[11] K. Neupane, D. B. Ritchie, H. Yu, D. A. N. Foster, F. Wang, and M. T. Woodside, Phys. Rev. Lett. **109**, 068102 (2012).
[12] K. Neupane, D. A. N. Foster, D. R. Dee, H. Yu, F. Wang, and M. T. Woodside, Science **352**, 239 (2016).
[13] K. Neupane, F. Wang, and M. T. Woodside, Proc. Natl. Acad. Sci. U.S.A. **114**, 1329 (2017).
[14] D. B. Ritchie and M. T. Woodside, Curr. Opin. Struct. Biol. **34**, 43 (2015).
[15] J. D. Bryngelson and P. G. Wolynes, J. Phys. Chem. **93**, 6902 (1989).
[16] J. N. Onuchic and P. G. Wolynes, Curr. Opin. Struct. Biol. **14**, 70 (2004).
[17] K. A. Dill and J. L. MacCallum, Science **338**, 1042 (2012).
[18] M. T. Woodside, W. M. Behnke-Parks, K. Larizadeh, K. Travers, D. Herschlag, and S. M. Block, Proc. Natl. Acad. Sci. U.S.A. **103**, 6190 (2006).
[19] M. T. Woodside, P. C. Anthony, W. M. Behnke-Parks, K. Larizadeh, D. Herschlag, and S. M. Block, Science **314**, 1001 (2006).
[20] See Supplemental Material at http://link.aps.org/supplemental/10.1103/PhysRevLett.121.018102 for Figs. S1–S6, Table S1, and Supporting Experimental Procedures, which includes Refs. [21–26].
[21] K. Neupane, H. Yu, D. A. N. Foster, F. Wang, and M. T. Woodside, Nucleic Acids Res. **39**, 7677 (2011).
[22] P. J. Elms, J. D. Chodera, C. J. Bustamante, and S. Marqusee, Biophys. J. **103**, 1490 (2012).
[23] W. J. Greenleaf, M. T. Woodside, E. A. Abbondanzieri, and S. M. Block, Phys. Rev. Lett. **95**, 208102 (2005).
[24] G.-M. Nam and D. E. Makarov, Protein Sci. **25**, 123 (2016).
[25] C. H. Reinsch, Numer. Math. **10**, 177 (1967).
[26] J. Lu and J. Nolen, Probab. Theory Relat. Fields **161**, 195 (2015).
[27] P. Cossio, G. Hummer, and A. Szabo, Proc. Natl. Acad. Sci. U.S.A. **112**, 14248 (2015).
[28] K. Neupane and M. T. Woodside, Biophys. J. **111**, 283 (2016).
[29] J. Kubelka, J. Hofrichter, and W. A. Eaton, Curr. Opin. Struct. Biol. **14**, 76 (2004).
[30] P. Hanggi, P. Talkner, and M. Borkovec, Rev. Mod. Phys. **62**, 251 (1990).
[31] M. T. Woodside, J. Lambert, and K. S. D. Beach, Biophys. J. **107**, 1647 (2014).
[32] D. E. Makarov, J. Chem. Phys. **143**, 194103 (2015).
[33] A. P. Manuel, J. Lambert, and M. T. Woodside, Proc. Natl. Acad. Sci. U.S.A. **112**, 7183 (2015).
[34] D. A. N. Foster, R. Petrosyan, A. Pyo, A. Hoffmann, F. Wang, and M. Woodside, Biophys. J. **114**, 1657 (2018).
[35] R. B. Best and G. Hummer, Proc. Natl. Acad. Sci. U.S.A. **107**, 1088 (2010).
[36] C. Hyeon and D. Thirumalai, J. Am. Chem. Soc. **130**, 1538 (2008).
[37] K. Neupane, A. P. Manuel, J. Lambert, and M. T. Woodside, J. Phys. Chem. Lett. **6**, 1005 (2015).
[38] D. Chandler, J. Chem. Phys. **68**, 2959 (1978).
[39] A. M. Berezhkovskii and D. E. Makarov, J. Chem. Phys. **148**, 201102 (2018).
[40] I. Popa, J. M. Fernández, and S. Garcia-Manyes, J. Biol. Chem. **286**, 31072 (2011).
[41] N. D. Socci, J. N. Onuchic, and P. G. Wolynes, J. Chem. Phys. **104**, 5860 (1996).
[42] D. K. Klimov and D. Thirumalai, Phys. Rev. Lett. **79**, 317 (1997).
[43] R. B. Best and G. Hummer, Phys. Rev. Lett. **96**, 228104 (2006).

[44] M. Jacob, M. Geeves, G. Holtermann, and F. X. Schmid, Nat. Struct. Mol. Biol. **6**, 923 (1999).
[45] T. Cellmer, E. R. Henry, J. Hofrichter, and W. A. Eaton, Proc. Natl. Acad. Sci. U.S.A. **105**, 18320 (2008).
[46] K. Neupane, A. P. Manuel, and M. T. Woodside, Nat. Phys. **12**, 700 (2016).
[47] A. N. Gupta, A. Vincent, K. Neupane, H. Yu, F. Wang, and M. T. Woodside, Nat. Phys. **7**, 631 (2011).
[48] E. Evans and K. Ritchie, Biophys. J. **72**, 1541 (1997).
[49] O. K. Dudko, G. Hummer, and A. Szabo, Phys. Rev. Lett. **96**, 108101 (2006).

SUPPORTING MATERIAL FOR

Measuring the velocity along transition paths during the folding of single biological molecules

Krishna Neupane, Noel Q. Hoffer, M.T. Woodside

Department of Physics, University of Alberta, Edmonton AB, T6G 2E1, Canada

SUPPORTING FIGURES

SUPPORTING TABLE

SUPPORTING EXPERIMENTAL PROCEDURES

SUPPORTING FIGURES

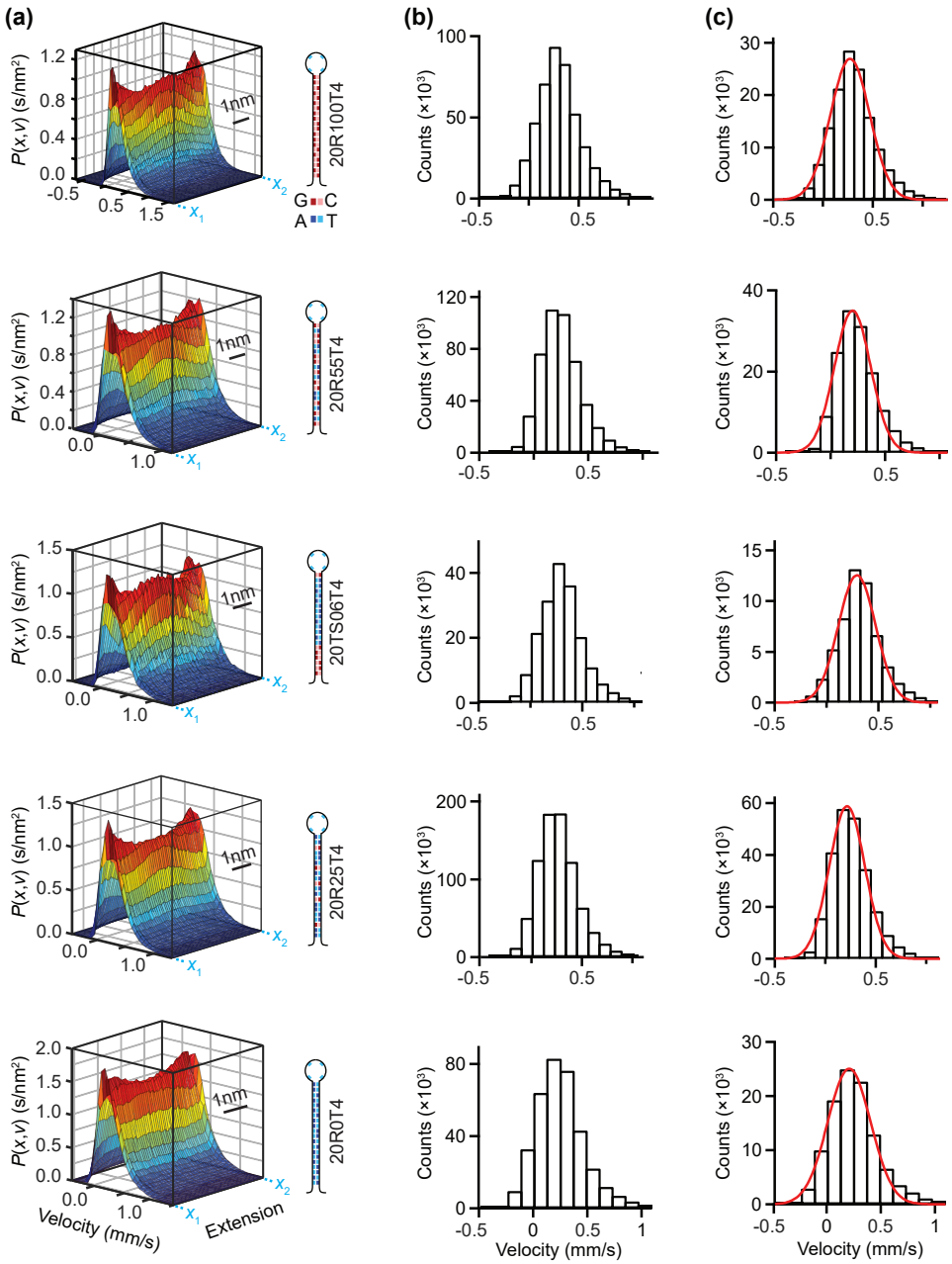

Figure S1: Transition-path velocity distributions. (a) Probability density for the velocity as a function of position within the barrier region for different hairpins. Inset: hairpin sequences. (b) The distribution of velocities observed at all positions in the barrier region is close to Gaussian for each hairpin. (c) Fitting the distribution of velocities observed at the barrier peak to a Gaussian yields *D*.

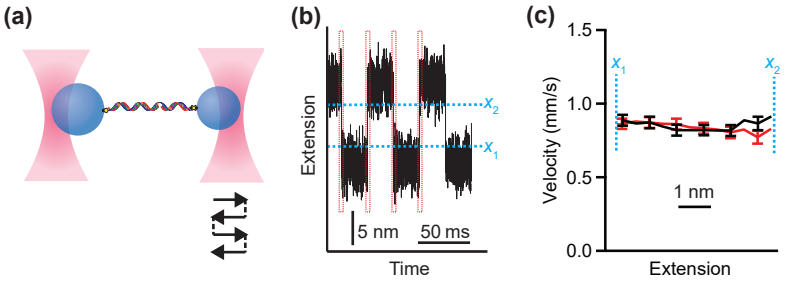

Figure S2: Measurements of reference construct without hairpins. (a) To test the effects of the beads and handles on the experimental results, a DNA tether without any hairpin was held at ~14 pN and one of the traps was jumped abruptly back and forth to cause the extension of the construct to change by an amount equal to the extension change in the folding of the hairpin 30R50/T4, as in Fig 2(a). (b) The "transitions" of the reference construct (red boxes) were extracted from the resulting extension trajectory. (c) The average velocity profile along the "transitions" for the reference construct for "folding" (black) and "unfolding" (red) was measured from 51,700 transitions. Error bars represent standard error of the mean.

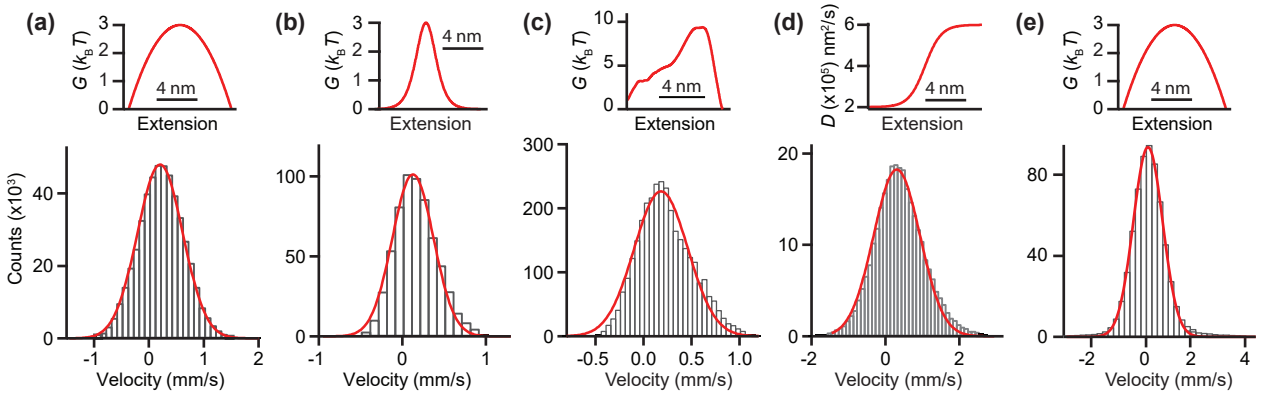

Figure S3: Simulated transition-path velocity distributions. The factors contributing to skew in the transition-path velocity distribution were explored using Brownian dynamics simulations. (a) Simulations of transitions over an harmonic barrier (inset) with constant *D* yield a Gaussian distribution with skew ~0, as expected. (b) Simulations using an anharmonic Eckart barrier (inset) with constant *D* yield a skewed distribution (here, skew ~0.4). (c) Simulations using the barrier measured for hairpin 30R50/T4 (inset) with constant *D* yield a slight skew (~0.2). (d) Simulations using an harmonic barrier as in (a) but with a sigmoidal *D*(*x*) (inset) yield skew (here, ~0.3). (e) Simulations including two types of transition paths having harmonic barriers of the same height (inset) but *D* differing by a factor of 5 yield skew (here, ~1); the faster transition path was occupied 1/6th of the time.

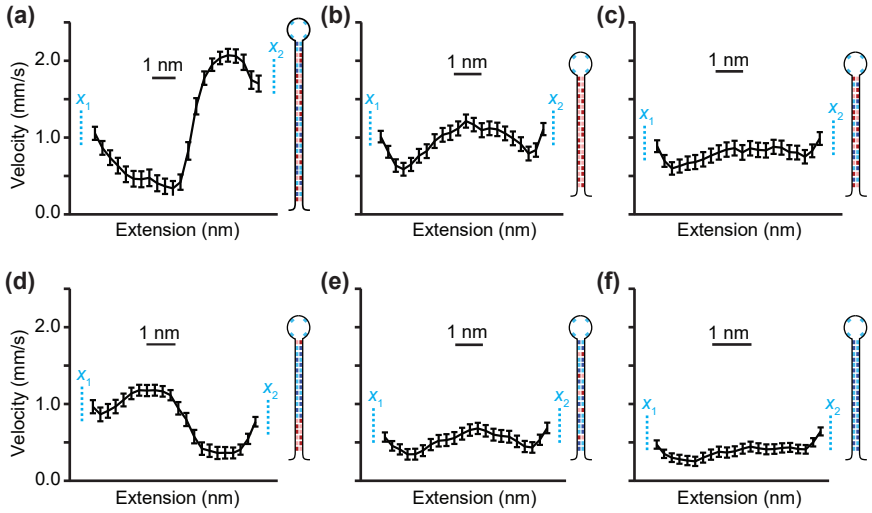

Figure S4: Simulated velocity profiles. The average transition-path velocity profiles expected from the experimentally measured energy landscapes under the assumption of constant *D* were determined from Brownian dynamics simulations for hairpins (a) 30R50/T4, (b) 20R100/T4, (c) 20R55T/4, (d) 20TS06/T4, (e) 20R25/T4, and (f) 20R0/T4. The simulated profiles share some qualitatively similar features with the observed velocity profiles (Fig 3) while differing in detail, suggesting that the observed profiles reflect position-dependence in *D*. Error bars represent standard error of the mean.

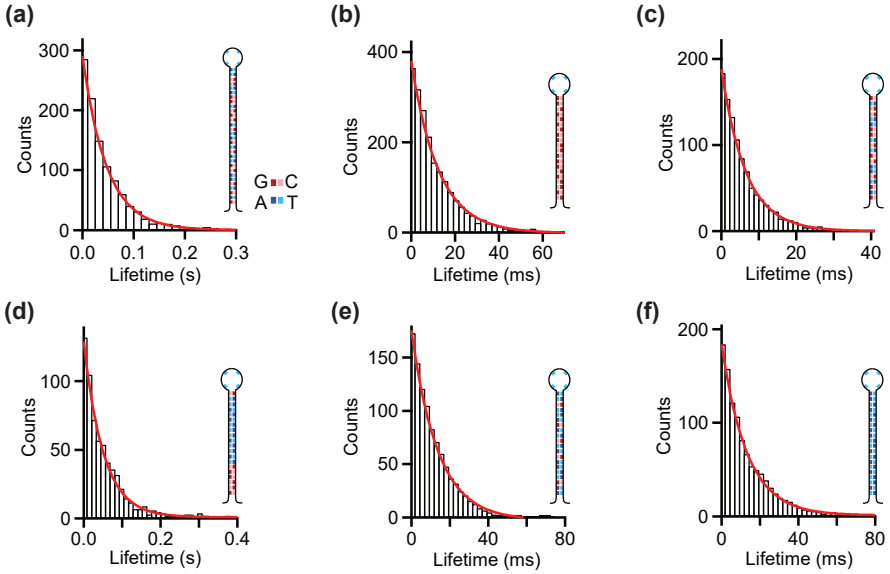

Figure S5: Rate measurements. Folding rates were determined from single-exponential fits (red) to the distribution of unfolded-state lifetimes (black) measured directly from extension trajectories. Representative examples are shown for hairpins (a) 30R50/T4, (b) 20R100/T4, (c) 20R55T/4, (d) 20TS06/T4, (e) 20R25/T4, and (f) 20R0/T4. The same analysis applied to folded-state lifetimes yielded the unfolding rates.

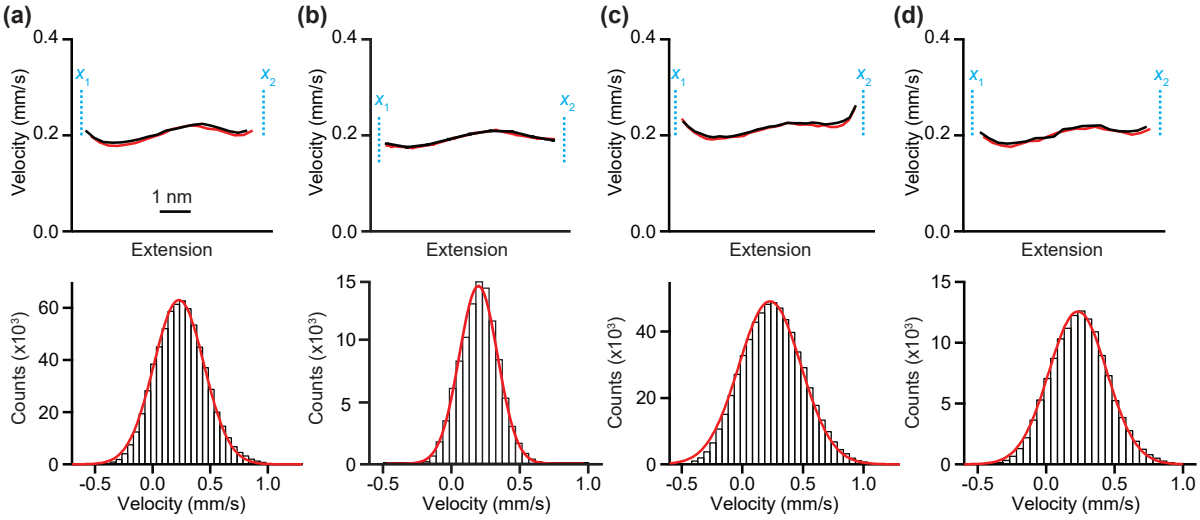

Figure S6: Effects of smoothing on velocity profiles. The velocity profiles (upper panels) were similar for different smoothing protocols: (a, b) smoothing spline with respectively $S = 0.7$ and $S = 1$, (c) Savitsky-Golay filter, (d) boxcar filter. Velocity distributions (lower panels) were qualitatively similar for similar amounts of smoothing (a, c, d).

SUPPORTING TABLE

Table S1. Observed rates, transition-state theory rates, and thermal velocities. Errors represent standard error on the mean.

DNA Hairpin	v_{th} ($\times 10^7$ mm/s)	k_f (s^{-1})	k_u (s^{-1})	k_f^{TST} ($\times 10^6$ s^{-1})	k_u^{TST} ($\times 10^6$ s^{-1})	N
30R50/T4	1.0 ± 0.1	22 ± 5	21 ± 4	2.3 ± 0.5	2.3 ± 0.5	32192
20R100/T4	1.4 ± 0.3	83 ± 1	109 ± 6	8 ± 2	11 ± 3	25144
20R55/T4	1.4 ± 0.3	133 ± 7	166 ± 3	18 ± 5	23 ± 7	36540
20TS06/T4	1.8 ± 0.7	16 ± 2	14 ± 1	4 ± 2	3 ± 1	8776
20R25/T4	1.4 ± 0.3	80 ± 3	91 ± 5	15 ± 4	17 ± 5	45833
20R0/T4	1.5 ± 0.4	65 ± 1	89 ± 5	70 ± 20	100 ± 30	8498

SUPPORTING EXPERIMENTAL PROCEDURES

Sample preparation and measurement: DNA hairpins connected at each end to double-stranded (ds) DNA handles were prepared as described previously [18,19]. Briefly, an oligonucleotide containing the hairpin sequence separated by abasic sites from a 5′ ligation overhang and a 3′ priming sequence was used to create a kilobase-long dsDNA handle with the hairpin on one end via autosticky PCR. The ligation overhang was used to ligate the PCR product to another kilobase-long dsDNA handle with a complementary overhang. The resultant construct was attached to 600- and 820-nm polystyrene beads via biotin/avidin and dioxigenin/anti-digoxigenin pairs, respectively, to generate 'dumbbells' for trapping (Fig 2(a)). Hairpin constructs were incubated at ~ 100 pM with 250 pM polystyrene beads to form dumbbells. Dumbbells were diluted to ~ 500 fM in 50 mM MOPS, pH 7.0, with 200 mM KCl and oxygen scavenging system (8 mU/μL glucose oxidase, 20 mU/μL catalase, 0.01% w/v D-glucose) to prevent oxidative damage from the traps, before insertion into a sample cell for the optical trap.

All samples were measured in a dual-trap optical tweezers apparatus described previously [21]. DNA hairpin measurements were made at equilibrium at a force near $F_{1/2}$, the force at which the occupancies of the folded and unfolded states were similar, under conditions of constant trap separation with high trap stiffness (0.75–1.1 pN/nm in one trap, and 0.56–0.63 pN/nm in the other). The force was not kept constant during the measurements, in order to avoid the artifacts that arise from feedback loops [22] as well as the reduced time resolution caused by passive force clamps [23]; it varied by ± 0.7–1 pN around $F_{1/2}$. Data were sampled at 125–512 kHz and filtered online at the Nyquist frequency. Note that the measurement conditions were such that the kinetic artifacts that arise from linking molecules to the handles and beads [24,27] are expected to be minimal [28]. Reference constructs were measured at a force near 14 pN, using the same trap stiffnesses and sampling rates as for the hairpins. One of the traps was moved abruptly to produce a length change in the tether similar to the length change observed when hairpin 30R50/T4 unfolded.

Velocity analysis: Transitions were identified as those parts of the trajectories traversing between the boundaries x_1 and x_2 separating respectively the folded and unfolded states from the barrier region. The barrier region was defined as the middle 2/3 of the distance traversed between F and U, Δx_{UF}), so that $x_1 = x_F + (1/6)\Delta x_{UF}$ and $x_2 = x_U - (1/6)\Delta x_{UF}$, where x_F and x_U are the positions of the folded and unfolded states, respectively (Fig. 2(b)). The velocity along each transition path was determined by numerical differentiation of the extension as a function of time. Because differentiation amplifies noise, however, we first smoothed the extension trajectories using a smoothing spline interpolation [25]. This approach finds the spline $g(t)$ that minimizes $\int(g'')^2 dt$ along the transition path, subject to the condition $\Sigma_i[(g(t_i) - x_i)/\sigma]^2 \leq S$, where x_i is the extension at a given point i, $g(t_i)$ is the value of the spline at that point, σ is the average standard deviation of the extension arising from fluctuations, and S is the smoothing factor. The smoothing was varied adaptively to account for the different average velocities of different transitions, ensuring that fast transitions were not over-smoothed and slow transitions were not under-smoothed. S was chosen for each transition such that the difference between the average velocity of the smoothed and unsmoothed transitions was kept below ~20% for each transition. The robustness of the results with respect to the choice of S was tested by repeating the analysis with constant S equal to the maximum value used in the adaptive smoothing algorithm ($S = 0.7$), as well as at $S = 1$; the resulting velocity profiles were qualitatively similar, differing primarily in

the average velocity (illustrated in Fig S6(a) and (b) for hairpin 30R50/T4), which decreased as the amount of smoothing increased. The results also did not depend on the type of smoothing filter used, as tested by reanalyzing the data using Savitsky-Golay and boxcar filters with comparable levels of smoothing (illustrated in Fig S6(c) and (d) for hairpin 30R50/T4).

We note that the extension change observed in these measurements was reduced from the value observed in constant-force measurements [18] owing to the compliance of the traps and handles, which reduces the distance travelled by the beads compared to the extension change in the hairpin [23]. The observed velocities of the beads were therefore multiplied by the compliance-correction factor appropriate for each hairpin to recover the velocity of the hairpin ends.

Brownian dynamics simulations: Brownian dynamics simulations were performed using the method described by Lu and Nolan [26], wherein the trajectories of transition paths are found by iteratively solving the Itô stochastic differential equation. The simulated trajectories were then analyzed as done for the experimental trajectories. The simulations for Fig. S3 used the potential landscapes shown in the insets, except for Fig. S3(d), where the same harmonic potential as in Fig S3(a) was used. The diffusion coefficient was $D = 2 \times 10^5$ nm^2/s for the simulations in Fig. S3(a–c). For Fig. S3(d), $D(x)$ was taken to be the logistic function shown in the inset; for Fig. S3(e), the two types of transition paths had diffusion coefficients $D_1 = 2 \times 10^5$ nm^2/s and $D_2 = 1 \times 10^6$ nm^2/s. The simulations for Fig. S4 used the energy landscapes measured previously for each hairpin [13], with a constant D given by the average of the values listed in Table 1.

Transmission factor estimates: The estimates of κ from Eqs. 2 and 3 and from Kramers' theory depend on estimating the effective mass associated with the reaction coordinate, which here is the end-to-end extension, x. When a basepair folds or unfolds, only the portion of the hairpin that is unfolded moves under the applied load. Hence the effective mass at a given x should be the mass of the unfolded DNA at that x value. Since we evaluate v_{th} at the barrier top, $x^{\ddagger}$, the relevant mass is that of the number of basepairs unfolded at $x^{\ddagger}$ times the average molecular weight per basepair of 650 Da. Note that the handles and beads do not contribute to the reaction mass because the measurements are done in the low-artefact limit where the observed hairpin kinetics (rates, average transition-path times and velocities) are little-changed by linking the hairpin to the beads. Including the handle/bead masses in the reaction mass would lead to the unphysical result that κ would vary by orders of magnitude if the bead mass were reduced to 0 even though the observed dynamics, being close to the intrinsic dynamics of the hairpin, remained effectively unchanged.